Diffusion Mechanism of the Sodium-Ion Solid Electrolyte Na_3PS_4 and Potential Improvements of Halogen Doping

De Klerk, Niek J J; Wagemaker, Marnix

DOI
10.1021/acs.chemmater.6b00698

Publication date
2016

Document Version
Accepted author manuscript

Published in
Chemistry of Materials

Citation (APA)
De Klerk, N. J. J., & Wagemaker, M. (2016). Diffusion Mechanism of the Sodium-Ion Solid Electrolyte Na_3PS_4 and Potential Improvements of Halogen Doping. *Chemistry of Materials*, *28*(9), 3122-3130. https://doi.org/10.1021/acs.chemmater.6b00698

The diffusion mechanism of the Na-ion solid electrolyte Na_3PS_4 and potential improvements of halogen doping

Niek J.J. de Klerk and Marnix Wagemaker*

Faculty of Applied Sciences, Delft University of Technology, The Netherlands

E-mail: m.wagemaker@tudelft.nl

Abstract

DFT MD-simulations were performed on cubic and tetragonal Na_3PS_4. The MD-simulations show that the Na-conductivity based on the predicted self-diffusion is high in both the cubic and tetragonal phase. Higher Na-ion conductivity in Na_3PS_4 can be obtained by introducing Na-ion vacancies. Just 2% vacancies results in a conductivity of 0.2 S/cm, which is an order of magnitude larger than the calculated conductivity of the stoichiometric compound. MD-simulations of halogen doped cubic Na_3PS_4 suggest a practical route to introduce vacancies, where Br-doping is predicted to result in the highest bulk conductivity. Detailed investigation of the Na-ion transitions during the MD-simulation reveals the role of vacancies and phonons in the diffusion mechanism. Furthermore, the orders of magnitude difference between the MD-simulations and experiments suggest that macroscopic conductivity can be significantly increased by reducing the grain boundary resistance.

Introduction

Nowadays the application of Li-ion batteries is widespread, powering mobile phones, laptops and electric cars. With the current growth rate the world's lithium resources could be depleted within 65 years,[1] not yet considering the potential use of Li-ion batteries for large-scale storage of renewable energy sources. Already decades ago the larger sodium abundance has motivated the development of materials for Na-ion batteries.[2–5] Especially for static large scale application, as required for the storage of renewable energy, the lower costs of Na-batteries may outweigh the lower energy density.[2] Both for Li-ion and Na-ion batteries the flammability of liquid electrolytes poses a safety risk encouraging the development of solid electrolytes.[6–9] An additional advantage of solid electrolytes is a potentially higher percentage of active material in the battery increasing the specific energy density, the ability to develop versatile geometries,[10] and stability in excess of 10000 cycles.[11] At present Na-ion solid state batteries, applied for static large scale storage, typically use β"-alumina as solid electrolyte operating at temperatures above 270°C.[4] For this material conductivities between 0.1 and 0.001 S/cm have been reported at room temperature.[4] However, the synthesis of β"-alumina requires temperatures above 1200°C, and even higher temperatures to lower the grain boundary resistance, making these systems inherently expensive. Recently Udovic et al.[12] have reported on $Na_2B_{12}H_{12}$, which is synthesised more easily, resulting in conductivities in the order of 0.1 S/cm above 270°C, however, with a relatively low room temperature conductivity of 10^{-6} S/cm. Sulphur based Na-ion solid electrolytes offer promising room temperature conductivities,[13] of which glass-ceramic Na_3PS_4 doped with Si currently has the highest reported conductivity reaching $7.4 * 10^{-4}$ S/cm at room temperature.[14] The tetragonal phase of Na_3PS_4 has been known as a sodium-conductor for more than 20 years.[15] Na_3PS_4 has gained renewed attention since Hayashi et al.[13] synthesised a room temperature stable glass ceramic phase showing a Na-conductivity of $2 * 10^{-4}$ S/cm. Since then the highest reported conductivities for this material are $4.6 * 10^{-4}$ S/cm,[16] and $7.4 * 10^{-4}$ S/cm with 6% Si-doping.[14] Although high conductivity is an important prerequisite for electrolyte

materials, good electrolyte-electrolyte and electrode-electrolyte contacts are an additional prerequisite for efficient charge transport in solid state batteries. For Na_3PS_4 it has been shown that good electrode-electrolyte contact can be obtained using cold pressing,[13] in contrast to β"-alumina that requires sintering at 1800°C to obtain good solid-solid contacts.[13] Yubuchi et al. demonstrated that Na_3PS_4 can be prepared via a liquid-phase reaction,[17] which can lead to even better electrode-electrolyte contacts.

The present work aims at revealing the diffusion mechanism in Na_3PS_4, based on which potential routes to increase the Na-ion conductivity are investigated by modelling the diffusion employing density functional theory (DFT) molecular dynamics (MD) simulations. For both the cubic and tetragonal phases of Na_3PS_4 high bulk self-diffusion is predicted, in both phases uncovering a vacancy mediated Na-ion transport mechanism. The modelling indicates that increasing the amount of vacancies, for instance achieved by halogen doping, may further enhance the Na-ion conductivity of this promising Na-ion solid electrolyte material.

Methods

DFT-calculations were performed using the GGA approach with the PAW-PBE basis set of VASP[18] and a cut-off energy of 280 eV. For the minimisation of Na_3PS_4 a single unit cell was used, and a k-point mesh of 4x4x4. For the minimisation of the other compositions a 2x2x2 super cell was used, with a k-point mesh of 2x2x2. For all the MD-calculations a 2x2x2 super cell was used, and a k-point mesh of 1x1x1 was used to reduce calculation time. The time between MD-steps was 2 femtoseconds, and the total simulation time was between 40 and 100 picoseconds. The MD-simulations were performed in the NVT-ensemble, with velocity scaling at every time-step. In all cases an equilibration time of 2.5 picoseconds was applied, to allow the system to reach equilibrium during the MD-simulations. Based on the MD-simulations the jump rates between the different crystallographic sites in the cubic crystals has been determined. To locate the crystallographic position of a Na-ion during the

MD-simulation the distance of a Na-ion to crystallographic distinct Na1(6b) and Na2(12d) sites was calculated. If the distance between the Na-ion and a crystallographic position is smaller than 1/8 of the unit cell length ($\sim$ 0.875 Å), corresponding to half the distance between neighbouring Na1- and Na2-sites, the Na-ion is assigned to the crystallographic position. In this way the crystallographic position of each Na-ion during the MD-simulation is known, and any transition towards another site can be distinguished.

Results

For Na_3PS_4 two crystal phases are known, a tetragonal phase,[15] and a cubic phase.[19] However, the differences between the two phases are small, the tetragonal phase being tetragonal distorted with respect to the cubic phase. The tetragonal phase of Na_3PS_4 crystallises in the space group $P\bar{4}2_1c$ (no. 114) with lattice parameters a = 6.9520 Å and c = 7.0757 Å,[15] while the cubic phase of Na_3PS_4 crystallises in the space group $I\bar{4}3m$ (no. 217) with lattice parameter a = 6.9965 Å.[19] The largest difference between the lattice parameters is 1.1%, and the volume difference is less as 0.2%. The only significant difference is in the positions of the Na-ions. In the tetragonal cell the cubic Na1(6b)-site splits into two Na-ion sites Na(2a) and Na(4d), where the latter is shifted approximately 0.5 Å with respect to its position in the cubic phase. For the cubic phase Na2(12d)-site occupancy is reported,[19] which are positioned between the Na1(6b)-sites, but present energy minimisations of this structure indicate that the Na2(12d)-sites are not stable. For both phases conductivities in the order of 10^{-6} S/cm have been reported in case of poor inter-particle contacts.[15,17] When the two phases are prepared in a similar way the two phases show similar conductivities.[20] Going from crystalline to glass-ceramic samples for the cubic phase results in a 30 times higher conductivity,[19] which if applicable to the tetragonal phase also should make Na-conductivities in the order of 10^{-4} S/cm possible. To test whether the small differences in crystal structure of the cubic and tetragonal phase have an influence on the Na-diffusivity MD-simulations

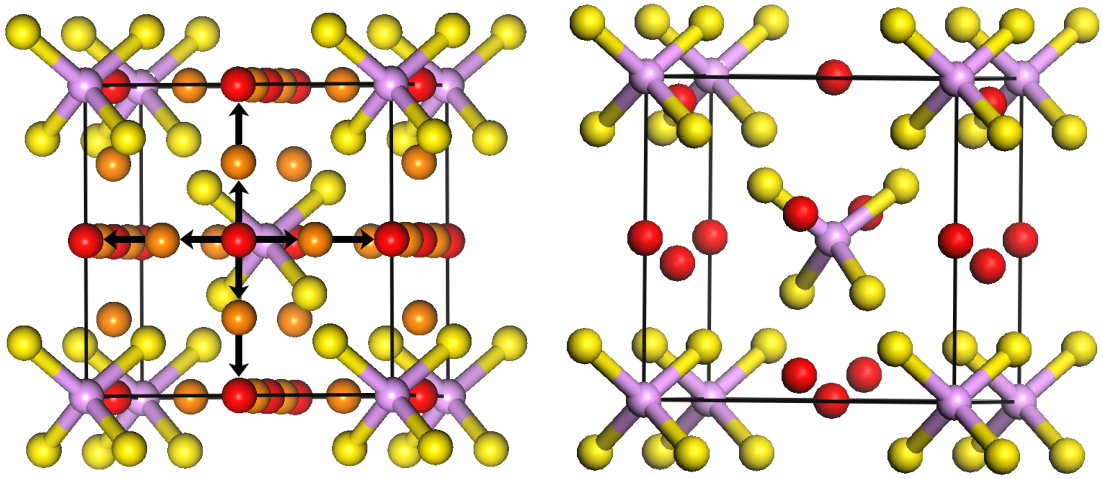

(a) (b)

Figure 1: (a) The unit cell of cubic Na_3PS_4, the P, S, Na1(6b)- and Na2(12d)-sites are represented by purple, yellow, red and orange, respectively, the proposed Na-pathway[19] is shown with arrows. (b) The unit cell of tetragonal Na_3PS_4, the P, S, and Na-sites are represented by purple, yellow, and red, respectively.

where performed on both phases. As a starting point for the calculations on the cubic phase the crystal structure reported by Tanibata et al.[19] was used, shown in Figure 1a. Relaxation of the reported structure, including a mixed Na1/Na2 occupancy,[19] resulted in migration of the Na-ions on the Na2(12d)-sites towards the nearest vacant Na1(6b)-site. Apparently, at zero Kelvin in stoichiometric Na_3PS_4 Na-ion occupancy of the Na2-site is unstable in comparison to the Na1-site, therefore further energy minimisations were performed with all Na-ions occupying the Na1-sites. For the tetragonal phase the crystal structure reported by Jansen et al.[15] was used as a starting point, shown in Figure 1b. After minimisation the energy of the tetragonal structure is 2 meV/atom lower compared to the energy of the cubic structure, in close agreement to the value of 5 meV/atom recently reported.[21] The lower energy of the tetragonal phase is consistent with experiments that have shown that the tetragonal structure is the stable phase at low temperatures, and that the cubic phase is more stable at high temperatures.[13] The only significant difference between the two phases at the start of the MD-simulations is the 0.5 Å displacement from the center of each face of 2/3 of the Na-ions in the tetragonal phase. The slightly different Na-positions do not lead

to significant differences in the Na-ion distributions during the MD-simulations, as shown in Figure 2. In Figures 2a and 2b the Na-ion distribution during a 100 ps. MD-simulation for stoichiometric Na_3PS_4 are shown, reflecting almost no Na-ion mobility between different Na1(6b)-sites at the time-scale of the MD-simulation. The Na-ions mostly vibrate around their original positions, and no transition paths between neighbouring Na-sites are observed. Calculations on defect formation energies in the closely related compound Na_3PSe_4 have shown that the formation energy of Na-vacancies is two times lower than formation energies of other common defects.[22] This in combination with the small amount of impurities present in the starting compounds[14,16] suggests that small amounts of Na-vacancies are present in Na_3PS_4, the impact of which will be investigated by introducing Na-vacancies in the MD-simulations. When 1 Na-atom is removed from the 2x2x2 super cell, corresponding to a composition of $Na_{2.94}PS_4$, the Na-ion mobility increases drastically as demonstrated in Figures 2c and 2d. For both the cubic and tetragonal phases the $Na_{2.94}PS_4$ composition shows a broad Na-ion distribution around the Na1(6b)-sites, which are interconnected through the Na2(12d)-sites, consistent with the proposed pathway based on the Maximum Entropy Method applied to powder XRD data.[19] The effect of the vacancy concentration on Na-ion conductivity was studied by systematically varying the vacancy concentration as shown in Table 1. For all stoichiometries Na_xPS_4 with x <2.94 the super cell was optimised resulting in minor changes of the lattice parameters, all within 1% from the experimental value. For both phases the crystal structure became unstable during MD-simulations at the composition of $Na_{2.25}PS_4$, indicating the maximum vacancy concentration that can be achieved while keeping the stable crystal structure is less than 25%.

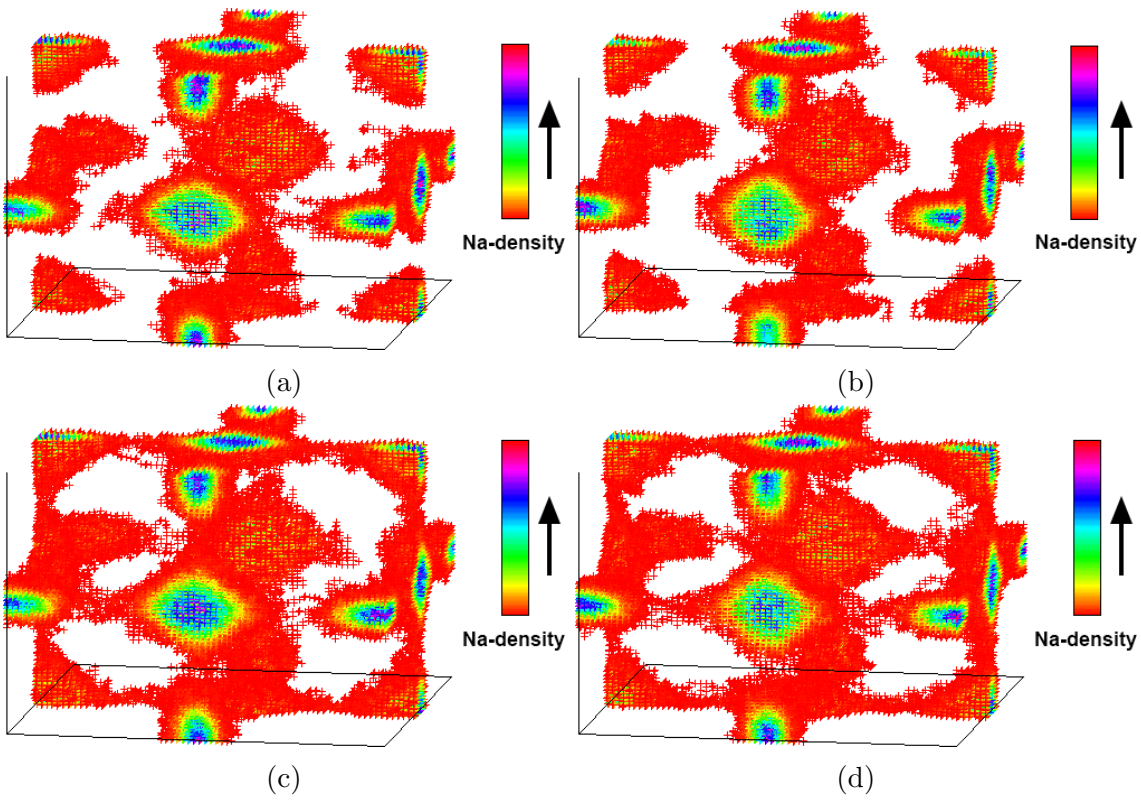

Figure 2: The Na-distribution during a 100 ps. MD-simulation at 525 K for (a) cubic Na_3PS_4, (b) tetragonal Na_3PS_4, (c) cubic $Na_{2.94}PS_4$, and (d) tetragonal $Na_{2.94}PS_4$.

Diffusivity

From MD-simulations the tracer diffusivity (D^*) can be calculated using the definition for the tracer diffusion coefficient:[23]

$$D^* = \frac{1}{N2d} \sum_{i=1}^{N} \left(\frac{dr_i(t)}{dt} \right)^2 \tag{1}$$

where N is the total number of diffusing particles, d the dimensionality of the diffusion path (3 in this case), dt the simulation time, and $dr_i(t)$ the displacement of a single diffusing particle. By using the Nernst-Einstein equation the diffusivity can be related to the conductivity (σ):[24]

$$\sigma = \frac{ne^2z^2D}{kT} \tag{2}$$

where n is the particle density, e the elementary charge, z the ionic charge, D the diffusivity, k is Boltzmann's constant, and T the temperature in Kelvin. The results shown in Figure 3

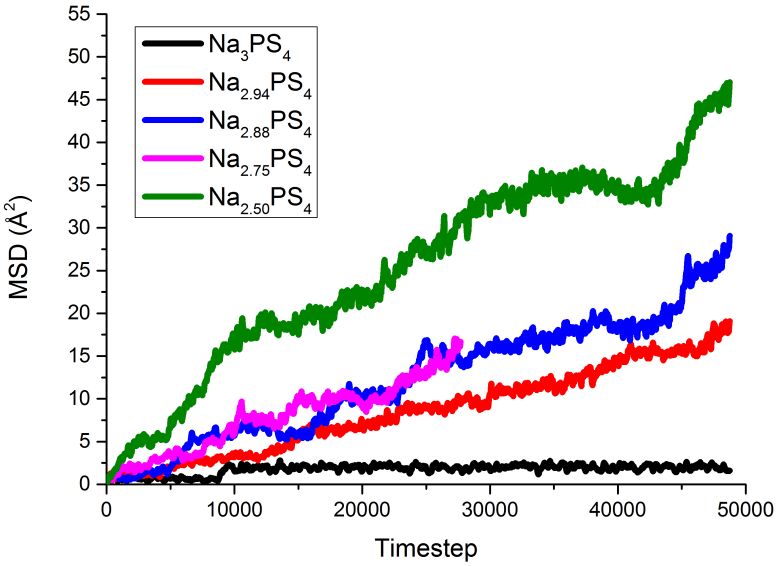

Figure 3: The MSD of Na during simulations with different compositions of Na_xPS_4 for the cubic phase at 525 K.

Table 1: Na-diffusivity and -conductivity for different compositions of Na_xPS_4 at 525 Kelvin based on the tracer diffusivity.

Composition	Phase	D* ($*10^{-6}$ cm^2/sec)	σ^* (S/cm)
Na_3PS_4	cubic	0.3	0.02
	tetragonal	0.1	0.01
$Na_{2.94}PS_4$	cubic	3.3	0.20
	tetragonal	2.3	0.14
$Na_{2.88}PS_4$	cubic	5.0	0.30
	tetragonal	5.4	0.33
$Na_{2.75}PS_4$	cubic	5.0	0.29
	tetragonal	8.1	0.47
$Na_{2.50}PS_4$	cubic	8.0	0.42
	tetragonal	8.2	0.43

and Table 1 show that introducing vacancies has a large influence on the conductivity. This is illustrated by comparing the Na-densities for Na_3PS_4 and $Na_{2.94}PS_4$ in Figure 2 where a vacancy concentration of 2% ($Na_{2.94}PS_4$) shows to have a large impact on the Na-diffusion. This is reflected by the large increase in the MSD when vacancies are introduced, for the cubic (Figure 3) as well as the tetragonal phase (Figure S1). Without vacancies the conductivity in the cubic and tetragonal phase are 0.02 and 0.01 S/cm, respectively, while a vacancy concentration of 2% ($Na_{2.94}PS_4$) results in an order of magnitude larger conductivity of 0.20 and 0.14 S/cm for the cubic and tetragonal phase respectively. Further increasing the vacancy concentration to 17% ($Na_{2.50}PS_4$) raises the conductivity to 0.42 and 0.43 S/cm for the cubic and tetragonal phase respectively. For the glass ceramic cubic Na_3PS_4 experimental conductivities in the order of 10^{-4} S/cm have been reported.[13,14,16,25] The results from the MD-simulations are two orders of magnitude higher in both phases. However, the experimentally measured macroscopic bulk conductivity includes diffusion over the grain boundaries and the electrode-electrolyte interface. Recently Nose et al. have shown that improving the contact between Na_3PS_4 particles can increase the conductivity by a factor of 2.[26] The 30 times increase in conductivity between crystalline and glass-ceramic samples[13] also indicates

that diffusion over grain boundaries is more sluggish than bulk diffusion in Na_3PS_4. This indicates that the large differences between simulated and experimental conductivities are primarily caused by grain boundary and interface resistivity. This suggests that improving the contacts between Na_3PS_4 particles could significantly increase the performance of electrolytes of this material. Although there are differences in the conductivities of the cubic and tetragonal phases, these are small and of the same order of magnitude as the error margin in the MD-calculations. The results shown in Figure 2 and in Table 1 predict that the cubic and tetragonal phases are equally good Na-ion conductors, and that the properties relevant to Na-diffusion are similar in both phases. This was confirmed by comparison of the mean jump rates and activation energies of the two phases, shown in the supporting information (Table S1). For brevity we will only describe the results for the cubic phase in the rest of this article.

Temperature dependence

The temperature dependence of the Na-ion diffusion was investigated by performing MD-simulations between 300 and 525 Kelvin for cubic $Na_{2.94}PS_4$ and $Na_{2.50}PS_4$. For $Na_{2.94}PS_4$ increasing the temperature showed to have a small effect, with the conductivity increasing from 0.17 S/cm at 300 K to 0.20 S/cm at 525 K. The effect of temperature is larger for $Na_{2.50}PS_4$, the conductivity went from 0.27 to 0.42 S/cm when increasing the temperature from 300 to 525 K. Because the lattice expansion with increasing temperature was not taken into account a MD-simulation with increased lattice parameters was also performed. The thermal volumetric expansion coefficient of Na_3PS_4 is unknown, however, for the related compound γ-Li_3PS_4 the volume expansion has been measured to be approximately 1.2% upon heating from 297 to 543 Kelvin.[27] Based on this we assume that the thermal volumetric lattice expansion of Na_3PS_4 is also small. Therefore MD-simulations were performed with 1% increased lattice parameters (3% volume expansion) for cubic $Na_{2.50}PS_4$ and $Na_{2.94}PS_4$ at 525 K. The expanded lattice resulted in an increased conductivity, for $Na_{2.94}PS_4$ σ^* amounting

10% and for $Na_{2.50}PS_4$ σ^* amounting 17%. Clearly, the lattice expansion upon increasing temperature has a significant effect on the conductivity.

Detecting transitions

Using the method described in the Methods section jumps between distinct crystallographic Na-sites can be extracted from the MD-simulations. Using equation 3 the mean jump rate (τ) of the Na-ions can be determined:

$$\tau = \frac{J}{Nt} \tag{3}$$

where J is the number of jumps between Na-sites, N the number of Na-ions in the super cell, and t the total simulation time. The mean jump rates for Na1→Na1-transitions and Na1→Na2-transitions are shown in Table 2. The most striking observation is the order of magnitude difference between the Na1→Na2 and Na1→Na1 mean jump rates, even when vacancies are present. This implies that in more than 90% of the cases a Na1→Na2 transition is followed by a backward Na2→Na1 transition, thus not contributing to (macroscopic) diffusion. Transition state theory can be used to calculate the activation energy (ΔE_A) with:[28]

$$\Delta E_A = -kT\ ln(\frac{\Gamma}{v_0}) \tag{4}$$

Where Γ is the hopping frequency and v_0 is the attempt frequency. Since macroscopic diffusion is caused by the Na1→Na1 transitions the Na1→Na1 jump rate is used as the hopping frequency and the Na1→Na2 jump rate as the attempt frequency. Although it is possible to determine the attempt frequency based on the lattice vibrations,[29] this is not a trivial procedure, and typically it is assumed to be on the order of 10^{13} sec^{-1}.[23] With the method of detecting transitions used at present, estimating the attempt frequency is straightforward, assuming the position of the transition state is known and sufficiently separated from the starting state and final state. In this case the attempt frequency is 12 to 25 times smaller

than the typically assumed 10^{13} sec^{-1}, where the latter would lead to severe overestimation of the activation energy. Table 2 shows that the introduction of vacancies results in

Table 2: Mean jump rates for the Na1→Na1-transition, mean jump rates for the Na1→Na2-transition, and the activation energy for Na1→Na1-transitions for different compositions of the cubic phase at 525 K.

Composition	mean Na1→Na1 jump rate ($*10^{10}$ sec^{-1})	mean Na1→Na2 jump rate ($*10^{10}$ sec^{-1})	ΔE_A Na1→Na1 (eV)
Na_3PS_4	0.09	41.56	0.28
$Na_{2.94}PS_4$	1.57	50.10	0.16
$Na_{2.88}PS_4$	3.28	60.60	0.13
$Na_{2.75}PS_4$	5.83	63.27	0.11
$Na_{2.50}PS_4$	7.97	79.38	0.10

an increased mean jump rate for both transitions. However, upon introducing 2% vacancies the mean Na1→Na1 jump rate increases by a factor of 17, while the mean Na1→Na2 jump rate only increases by a factor of 1.2. This effect is reflected in the activation energies for Na1→Na1 transitions, which show a reduction of 0.12 eV on going from no vacancies (Na_3PS_4) to 2% vacancies ($Na_{2.94}PS_4$). By adding more vacancies the activation energy decreases further, although the effect per vacancy becomes smaller. Experimentally activation energies between 0.20 and 0.28 eV have been reported, depending on the preparation procedure,[14,16] with more crystalline phases showing lower activation energies. The activation energies from the MD-simulations are very similar to the experimentally determined values, where the activation energy of Na_3PS_4 corresponds to the highest experimental value, and the activation energy based on 2% Na-vacancies is close to the lowest experimental activation energy. Using the mean jump rates the diffusivity (D_J) can be calculated using the Einstein-Smoluchowski equation:

$$D_J = \frac{\tau a^2}{2d} \tag{5}$$

Where τ is the mean jump rate, a is the distance between the sites (3.5 Å between Na1(6b)-sites), and d is the number of dimensions of the diffusion pathway. Since only the Na1→Na1-transitions contribute to macroscopic diffusion, the diffusivity is calculated based on the mean

jump rate of this transition. Using Equation 2 the conductivity based on the mean jump rates (σ_J) can also be calculated. When comparing the conductivities in Figure 4 significant

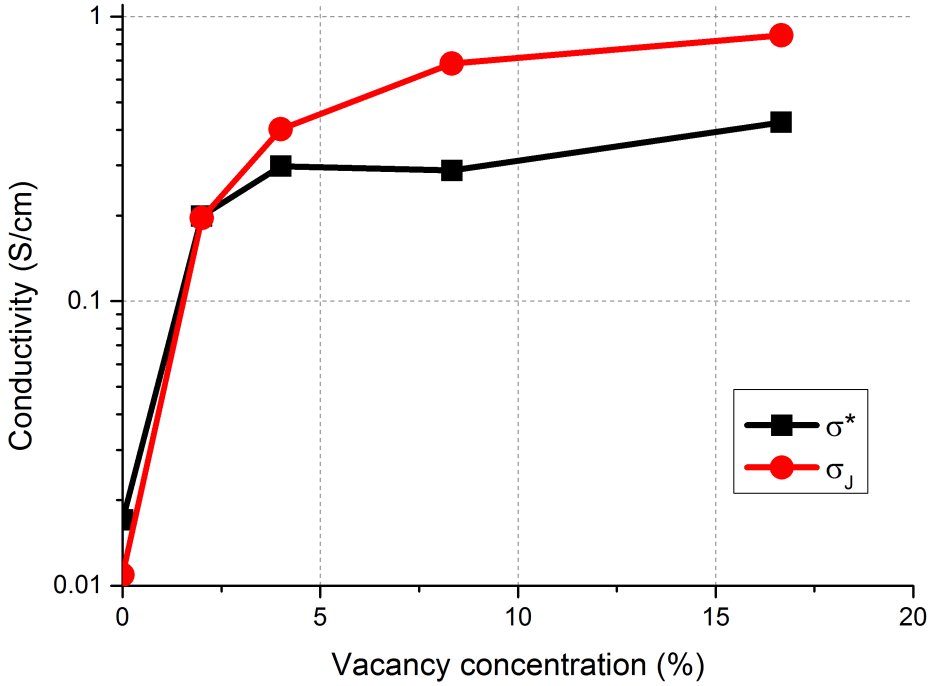

Figure 4: The conductivity, based on the tracer conductivity (σ^*) and on the mean Na1→Na1 jump rate (σ_J), versus vacancy concentration for the cubic phase at 525 K.

differences are observed between the conductivities based on the tracer diffusivity and the mean jump rate. This can be explained by the back and forth transitions that contribute to the jump rates, thereby increasing the conductivity, whereas for the calculation of the tracer diffusivity these cancel out. This can be quantified by the correlation factor (f), which is defined as $f = \frac{D^*}{D_J}$.[23] For the vacancy rich compositions both diffusivity and conductivity are larger when calculated based on the jump rates, therefore f<1, indicating that in the presence of vacancies Na-ions often jump back and forth between Na1(6b)-sites. Figure 4 suggests a relation between f and the vacancy concentration, however, we anticipate that this has no physical origin. At low vacancy concentrations on average the Na-ions perform only a few jumps during the simulations. Because the number of jumps is small, a jump to a previously visited site becomes less likely, and f will be overestimated. This effect is smaller

at high vacancy concentrations since then more jumps occur, increasing the chance of back and forth jumps, explaining the dependence of f on the vacancy concentration. In order to obtain reliable values of f at low concentrations much more jumps should be sampled. This was not attempted here because of the significantly longer computational times this would require.

Metastability of the Na2-site

Tanibata et al.[19] report partial occupancies in the cubic phase, the Na2(12d)-site having an occupancy of 10% and the Na1(6b)-site having an occupancy of 80%, determined by refinement of room temperature X-ray diffraction data. Because the multiplicity of the Na2(12d)-sites is twice that of the Na1(6b)-sites this implies that Na-ions on average spent 20% of their time on Na2-sites, and 80% of their time at Na1-sites. As mentioned earlier, relaxing a cubic structure with partial Na2-site occupancy towards its minimal energy results in migration of the Na-ions from the Na2-sites towards the Na1-sites, indicating that at zero Kelvin the Na2-site is unstable and thus unoccupied. At room temperature therefore, the Na2-occupancies must be due to transitions between neighbouring Na1-sites connected via Na2-sites, as indicated by the electron density derived from the maximum entropy method[19] and the average Na-ion density from the present MD-simulations in Figures 2c and 2d. The average Na2-site occupancies at finite temperatures can be extracted from the MD-simulations, the results of which are shown in Table 3. These indicate that an increasing number of vacancies, or equivalently a larger conductivity, induces a larger time spend on the Na2-site, consistent with the increasing Na1→Na2 jump rate in Table 2. The increased amount of time the Na-ions spend on the Na2-site does not imply that the Na2-site becomes stabilised by Na-vacancies. In Figure 2 it is visible that the Na-distribution around the Na1-sites broadens when Na-vacancies are introduced. At higher vacancy concentrations this effect becomes more pronounced, as shown in Figure S2. The increased Na2-occupancy can

thus be ascribed to larger Na-vibrations at the Na1-site, and a higher number of Na1→Na1-transitions. The metastability of the Na2-site is confirmed by the MD-simulations at different

Table 3: The percentages of time Na-ions spend at the Na2-site for different compositions of the cubic phase at 525 Kelvin.

Composition	% of time at Na2-site
Na_3PS_4	3.0
$Na_{2.94}PS_4$	5.3
$Na_{2.88}PS_4$	8.1
$Na_{2.75}PS_4$	10.8
$Na_{2.50}PS_4$	16.4

temperatures for cubic $Na_{2.94}PS_4$ and $Na_{2.50}PS_4$, in which the percentage of time spent at the Na2-site increases with temperature. For $Na_{2.94}PS_4$ at 300 Kelvin the percentage of time spent at Na2-sites is 2.9%, increasing to 4.1%, 4.7% and 5.3% at 375, 450 and 525 K, respectively. The percentage of time at the Na2-site for $Na_{2.50}PS_4$ is 13.1%, 14.7%, 15.7%, and 16.4% at 300, 375, 450 and 525 K, respectively. In Figure 5 the diffusion path of a single Na-ion is shown. The Na-ion vibrates around the Na1-sites most of the time, whereas in contrast the Na2-site is occupied very shortly during the transition. During the transitions between Na1-sites in Figure 5 the Na-ion passes through the Na2-site and no vibrations near the Na2-site are observed, further indicating that the Na2-site is not stable.

The transition mechanism

The rise in conductivity with increasing vacancy concentrations predicted by the MD-simulations indicates that diffusion proceeds through a vacancy mechanism. Note that a different mechanism seems to occur upon Si-doping ($Na_{3+3x}P_{1-x}S_4Si_x$ with x between 0 and 0.06)[14] which also leads to increased conductivities, due to interstitial Na-ions introduced upon Si-doping.[21] In contrast to the related Na_3PO_4 compound, where it has been reported that the Na-diffusion is mediated through the rotation of PO_4-groups (a paddle-wheel mechanism),[30,31] the present MD-simulations do not display rotating PS_4-groups in

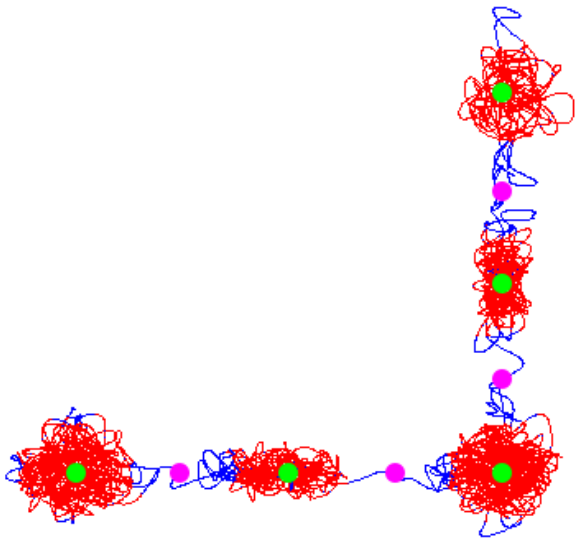

Figure 5: The diffusion path of a single Na-ion during the MD-simulation for cubic $Na_{2.94}PS_4$ at 525 K. The red and blue colors correspond to the atom residing at the Na1(6b)- and Na2(12d)-site, respectively, and green and pink dots correspond to the crystallographic Na1(6b)- and Na2(12d)-positions, respectively.

Na_3PS_4. Table 2 illustrates the high frequency of Na1→Na2-transitions, but less than 10% leads to Na1→Na1-transitions, the latter being responsible for bulk conductivity. To determine what is preventing Na1→Na1-transitions after a successful Na1→Na2-transition the conditions of three different case are investigated:

I Successful transition to a neighbouring Na1-site (contributing to bulk conductivity).

II No Na1→Na1 transition because the neighbouring site is already occupied.

III No Na1→Na1 transition for another reason.

The relative occurrence of each of these cases at different temperatures is shown for cubic $Na_{2.50}PS_4$ in Table 4. As expected raising the temperature increases the relative amount of successful Na1→Na1 transitions (case I). More surprisingly, it also shows an increase in failing transitions due to occupation of the destination Na1-site (case II), and a decrease in failing transitions for other reasons (case III). To investigate the mechanism behind this the

Table 4: Percentages of case I, II and III at different temperatures for cubic $Na_{2.50}PS_4$.

Temperature (K)	Case I (%)	Case II (%)	Case III (%)
300	6.8	50.6	42.6
375	8.5	57.3	34.3
450	10.5	62.2	27.3
525	10.2	69.7	20.1

radial distribution functions (RDF) for all the Na-atoms at the Na2-site were determined. By combining the RDF's of individual Na-atoms per case the average atomic surrounding of the Na-ions for each case can be determined by the RDF's. Based on the differences between the RDF's of the three cases it is possible to deduce what atomic surroundings are responsible for successful and failing transitions, thus providing insight in the transition mechanism. Independent of the crystal structure, composition, and temperature all MD-simulations display similar RDF's, indicating that in all present MD-simulations a similar diffusion mechanism takes place. To analyse differences between the RDF's for the three cases the MD-simulation of cubic $Na_{2.88}PS_4$ at 525 K was used, resulting in Na-Na, Na-P and Na-S RDF's for each case as shown in Figure 6. As a consequence of the higher occupancy of neighbouring Na-sites case II (no transition because the neighbouring Na-site is occupied) shows a slightly larger average Na-ion occupancy in the first 3.5 Å compared to the other two cases as shown in Figure 6a. There is no significant difference between the Na-distributions for case I and case III in the first few Ångstroms, illustrating that this is not the only parameter preventing Na1→Na1-transitions. In Figure 6b the Na-S RDF is shown, displaying the most obvious differences between 3 and 4 Å. For successful transitions (case I) on average less S-atoms are located between 3 and 3.5 Å, which apparently shift to the range 3.5 to 4 Å, indicating a different atomic arrangement when a successful jump occurs. The Na-P RDF in Figure 6c shows a clear difference around 4 Å, for case I a single P-peak is observed here, while for the other cases two peaks are visible. This indicates that a prerequisite for a successful transition is that the Na-ion is in the centre of the nearest P-atoms, i.e. it is exactly at the crystallographic Na2-position. Concluding, the Na-P and

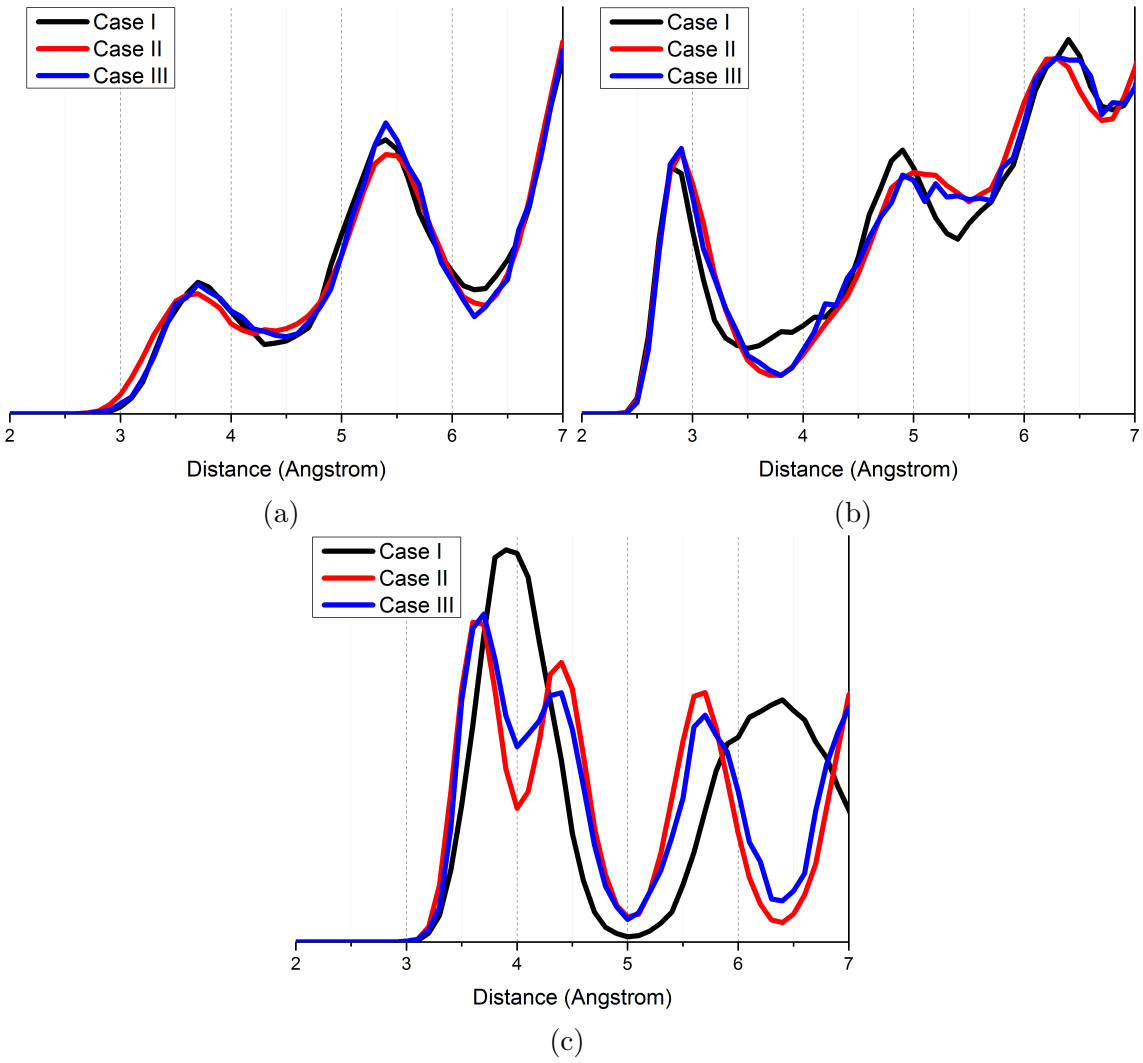

Figure 6: The (a) Na-Na, (b) Na-S and (c) Na-P RDF's between 2 and 7 Å for the three cases from the MD-simulation of cubic $Na_{2.88}PS_4$ at 525 K.

Na-S RDF's show that when a successful transition occurs there are less P and S atoms in the first 3.5 Å . The extra free volume around the Na-ion enlarges the window through which the ion must hop for a successful Na1→Na1-transition, indicating that opening of this window is vital for macroscopic diffusion. The better conductivity for expanded lattices can be explained by this effect. In the expanded lattice on average the windows will be larger which leads to the observed improved conductivity. The extra free volume has to be created by phonons within the crystal, which explains the changing ratio between case I and case III with increasing temperature. At higher temperatures more phonons are present, thus the window for a transition will be open more frequently, enhancing the Na1→Na1 transitions and hence the macroscopic diffusion.

Halogen doping in Na_3PS_4

The results from MD-simulations shown in Figure 4 indicate that introducing Na-vacancies into Na_3PS_4 will increase the bulk conductivity. In MD-simulations the vacancies can be introduced without charge compensation, however, in reality charge compensation is necessary when introducing vacancies. A straightforward way to introduce vacancies in Na_3PS_4 would be by replacing S atoms with halogen atoms, a commonly used approach in Li-sulphide materials.[32] DFT calculations on Na-argyrodite solid electrolytes have shown that upon doping with halogens the materials remain stable,[33] therefore we expect that doping with halogens is also possible for Na_3PS_4. To simulate the impact of halogen doping a 2x2x2 super cell of the cubic phase was built, in which two S atoms were replaced with halogen atoms charge compensated by removing two Na-ions, resulting in the composition $Na_{2.88}PS_{3.88}X_{0.12}$ (X = F, Cl, Br, I), corresponding to 4% Na-vacancies via halogen doping. Structural energy minimisations were performed for several configurations of Cl-atoms and Na-vacancies. To find the lowest energy configuration the Cl atoms were placed on nearest S-positions, as well as S-positions with the maximal distance within the 2x2x2 super cell. Na-vacancies were

positioned next to the Cl-atoms and as far from the Cl-atoms as possible. The resulting energies suggest that Cl-atoms prefer to be well distributed in the lattice, maximising their mutual distance, whereas Na-vacancies are preferably located next to the Cl-atoms. This lowest energy configuration was used as a starting point for relaxations of the other halogen dopants. After relaxation the cell parameters changed by less than 1% in all cases. MD-simulations for all halogen dopants were performed at 525 K, the resulting conductivities are compared to the cubic phase without charge compensation in Figure 7. The conduc-

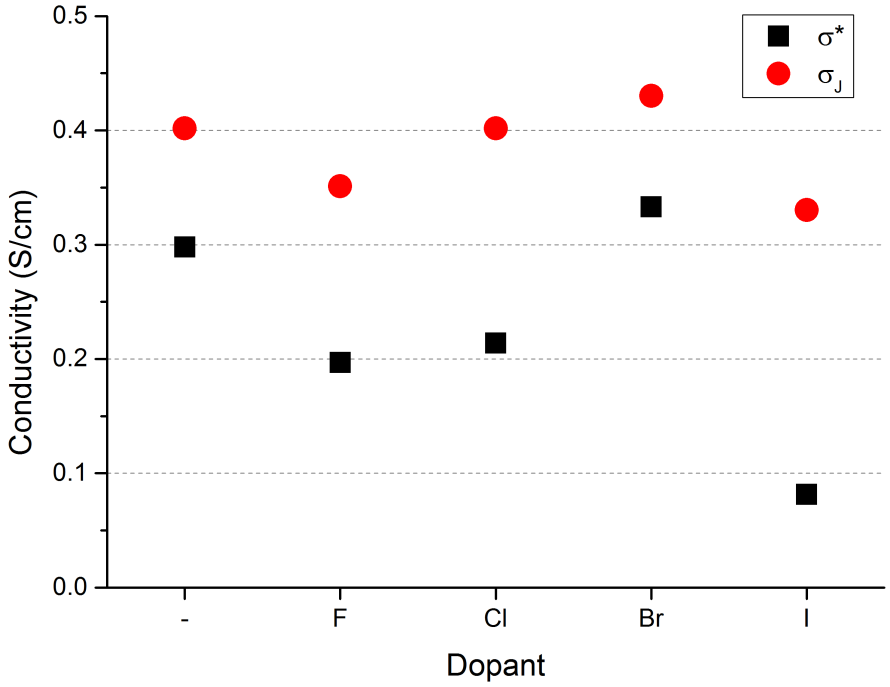

Figure 7: The conductivities for 4% Na-vacancy concentration without (-) and with halogen doping from MD-simulations of the cubic phase at 525 K based on the MSD (σ^*) and mean Na1→Na1 jump rates (σ_J).

tivities with halogen doping are comparable to the values for cubic $Na_{2.88}PS_4$. The Na-Na distribution changes slightly (shown in Figure S3), but other properties such as the mean jump rates, activation energy, and the occupancy of the Na2-site are comparable to the MD-simulation for cubic $Na_{2.88}PS_4$. This indicates that doping with halogens has the same effect in the DFT-MD simulations as the vacancies without charge compensation, and it is

concluded that doping with halogens may be a promising strategy to further improve the conductivity of Na_3PS_4. That the conductivity rises when going from F- to Cl- to Br-doping

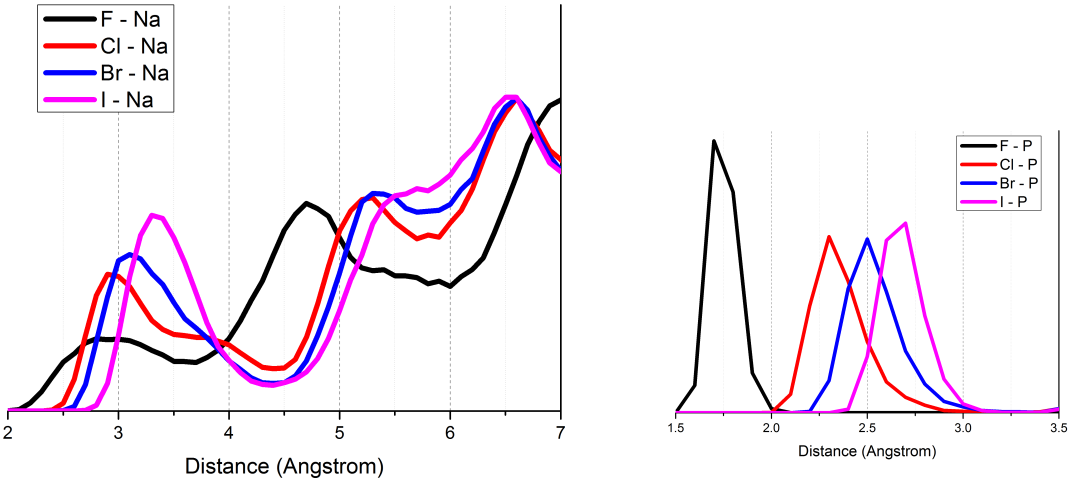

(a) (b)

Figure 8: The (a) X-Na distribution between 2 and 7 Å, and (b) the X-P distribution between 1.5 and 3.5 Å from the MD-simulation of cubic $Na_{2.88}PS_{3.88}X_{0.12}$ (X = F, Cl, Br, I) at 525 K.

indicates that a larger ionic radius of the dopant increases the conductivity of halogen-doped Na_3PS_4. However, the lower conductivity upon I-doping indicates that this trend does not continue beyond Br. To explain this the distribution functions for the different halogens are shown in Figure 8. The X-Na (X = F, Cl, Br, I) distributions in Figure 8a strongly depend on the halogen dopant. Upon increasing halogen ionic radius the first peak of the Na-distributions becomes more narrow, indicating that the Na-positions are better defined. The larger ionic radius also has an effect on the window through which a transition to the neighbouring Na1(6b)-site occurs, as shown in the X-P distributions in Figure 8b. With larger ionic radius the X-P distance increases, making the window through which diffusion occurs smaller, and Na1-Na1 transitions less likely to occur. These two mechanisms have opposite effects as a function of halogen ionic radius, with an apparent optimum effect on diffusion for Br-doping. Thereby the MD-simulations indicate that Br-doping should lead to the highest vacancy induced conductivity in Na_3PS_4.

Conclusions

DFT MD-simulations indicate that higher Na-ion conductivity in Na_3PS_4 can be obtained by introducing Na-ion vacancies. Just 2% vacancies results in an order of magnitude larger conductivity (compared to the stoichiometric compound), reaching 0.20 S/cm, and a reduction in the activation energy from 0.28 eV to 0.16 eV. MD-simulations of halogen doped cubic Na_3PS_4 suggest a practical route towards charge compensated vacancies to raise the conductivity of this material. A systematic variation of the halogen dopants indicates that all halogens can increase the conductivity by raising the Na-vacancy concentration, with Br-doping leading to the best results. Not only vacancies appear vital for microscopic diffusion, the MD-simulations indicate that free volume also plays a role in the transition mechanism. A large free volume induced by phonons enhances the chance for Na-ions to make a successful transition towards a neighbouring site. The MD-simulations also show that Na-conductivity in the cubic and tetragonal phase are similar, thus both phases of Na_3PS_4 are predicted to be highly conductive solid electrolytes. Furthermore, the orders of magnitude difference between the MD-simulations and experiments suggest that macroscopic conductivity can be significantly increased by reducing the grain boundary resistance, which is most likely one of the major bottlenecks towards high performance solid state batteries. The Na2(12d)-site in the cubic phase, connecting the occupied Na1(6b)-sites, shows to be metastable, and upon increased Na-ion conductivity the time averaged Na2-site occupancy increases with increasing vacancy concentrations and/or higher temperatures due to an increase in Na1$\rightarrow$Na1 transitions. Thereby present DFT-MD simulations reveal the diffusion mechanism, and potential routes towards larger Na-ion conductivities in Na_3PS_4.

Supporting information

Plot of the MSD, mean jump rates and activation energies for different compositions of the tetragonal phase, Na-density plots of cubic $Na_{2.88}PS_4$ and $Na_{2.50}PS_4$, and Na-Na RDF's from

simulations with halogen doping.

Acknowledgements

Financial support from the Advanced Dutch Energy Materials (ADEM) program of the Dutch Ministry of Economic Affairs, Agriculture and Innovation is gratefully acknowledged. The research leading to these results has received funding from the European Research Council under the European Union's Seventh Framework Programme (FP/2007-2013)/ERC Grant Agreement nr. [307161] of M.W.

References

(1) Zu, C.-X.; Li, H. Thermodynamic Analysis on Energy Densities of Batteries. *Energy Environ. Science* **2011**, *4*, 2614–2624.

(2) Slater, M. D.; Kim, D.; Lee, E.; Johnson, C. S. Sodium-Ion Batteries. *Adv. Funct. Mater.* **2013**, *23*, 947–958.

(3) Ellis, B. L.; Nazar, L. F. Sodium and Sodium-ion Energy Storage Batteries. *Curr. Opin. Solid State Mater. Sci.* **2012**, *16*, 168–177.

(4) Lu, X. C.; Xia, G. G.; Lemmon, J. P.; Yang, Z. G. Advanced Materials for Sodium-beta Alumina Batteries: Status, Challenges and Perspectives. *J. Power Sources* **2010**, *195*, 2431–2442.

(5) Sudworth, J. L. The Sodium/Sulphur Battery. *J. Power Sources* **1984**, *11*, 143–154.

(6) Takada, K. Progress and Prospective of Solid-state Lithium Batteries. *Acta Mater.* **2013**, *61*, 759–770.

(7) Knauth, P. Inorganic Solid Li Ion Conductors: An Overview. *Solid State Ionics* **2009**, *180*, 911–916.

(8) Thangadurai, V.; Weppner, W. Recent Progress in Solid Oxide and Lithium Ion Conducting Electrolytes Research. *Ionics* **2006**, *12*, 81–92.

(9) Anantharamulu, N.; Koteswara Rao, K.; Rambabu, G.; Vijaya Kumar, B.; Radha, V.; Vithal, M. A Wide-ranging Review on Nasicon Type Materials. *J. Mater. Sci.* **2011**, *46*, 2821–2837.

(10) Tatsumisago, M.; Hayashi, A. Sulfide Glass-Ceramic Electrolytes for All-Solid-State Lithium and Sodium Batteries. *Int. J. Appl. Glass Sci.* **2014**, *5*, 226–235.

(11) Li, J.; Ma, C.; Chi, M.; Liang, C.; Dudney, N. J. Solid Electrolyte: the Key for High-Voltage Lithium Batteries. *Adv. Energy Mater.* **2015**, *5*, n/a–n/a.

(12) Udovic, T. J.; Matsuo, M.; Unemoto, A.; Verdal, N.; Stavila, V.; Skripov, A. V.; Rush, J. J.; Takamura, H.; Orimo, S.-i. Sodium Superionic Conduction in $Na_2B_{12}H_{12}$. *Chem. Commun.* **2014**, *50*, 3750–3752.

(13) Hayashi, A.; Noi, K.; Sakuda, A.; Tatsumisago, M. Superionic Glass-ceramic Electrolytes for Room-temperature Rechargeable Sodium Batteries. *Nat. Commun.* **2012**, *3*, 856.

(14) Tanibata, N.; Noi, K.; Hayashi, A.; Tatsumisago, M. Preparation and Characterization of Highly Sodium Ion Conducting Na_3PS_4-Na_4SiS_4 Solid Electrolytes. *RSC Adv.* **2014**, *4*, 17120–17123.

(15) Jansen, M.; Henseler, U. Synthesis, Structure Determination, and Ionic Conductivity of Sodium Tetrathiophosphate. *J. Solid State Chem.* **1992**, *99*, 110–119.

(16) Hayashi, A.; Noi, K.; Tanibata, N.; Nagao, M.; Tatsumisago, M. High Sodium Ion Conductivity of Glass Ceramic Electrolytes with Cubic Na_3PS_4. *J. Power Sources* **2014**, *258*, 420–423.

(17) Yubuchi, S.; Hayashi, A.; Tatsumisago, M. Sodium-ion Conducting Na_3PS_4 Electrolyte Synthesized via a Liquid-phase Process Using *N*-Methylformamide. *Chem. Lett.* **2015**, *44*, 884–886.

(18) Kresse, G.; Hafner, J. Ab Initio Molecular Dynamics for Liquid Metals. *Phys. Rev. B* **1993**, *47*, 558–561.

(19) Tanibata, N.; Noi, K.; Hayashi, A.; Kitamura, N.; Idemoto, Y.; Tatsumisago, M. X-ray Crystal Structure Analysis of Sodium-Ion Conductivity in $94Na_3PS_4 \cdot 6Na_4SiS_4$ Glass-Ceramic Electrolytes. *Chem. Electro. Chem* **2014**, *1*, 1130–1132.

(20) Noi, K.; Hayashi, A.; Tatsumisago, M. Structure and Properties of the Na_2S-P_2S_5 Glasses and Glass Ceramics Prepared by Mechanical Milling. *J. Power Sources* **2014**, *269*, 260–265.

(21) Zhu, Z.; Chu, I.-H.; Deng, Z.; Ong, S. P. Role of Na^+ Interstitials and Dopants in Enhancing the Na^+ Conductivity of the Cubic Na_3PS_4 Superionic Conductor. *Chem. Mater.* **2015**, *27*, 8318–8325.

(22) Bo, S.-H.; Wang, Y.; Kim, J. C.; Richards, W. D.; Ceder, G. Computational and Experimental Investigations of Na-Ion Conduction in Cubic Na_3PSe_4. *Chem. Mater.* **2016**, *28*, 252–258.

(23) Van der Ven, A.; Ceder, G.; Asta, M.; Tepesch, P. D. First-principles Theory of Ionic Diffusion with Nondilute Carriers. *Phys. Rev. B* **2001**, *64*.

(24) Friauf, R. J. Correlation Effects for Diffusion in Ionic Crystals. *J. Appl. Phys.* **1962**, *33*, 494–505.

(25) Nagata, H.; Chikusa, Y. An All-solid-state Sodium-Sulfur Battery Operating at Room Temperature Using a High-sulfur-content Positive Composite Electrode. *Chem. Lett.* **2014**, *43*, 1333–1334.

(26) Nose, M.; Kato, A.; Sakuda, A.; Hayashi, A.; Tatsumisago, M. Evaluation of Mechanical Properties of Na_2S-P_2S_5 Sulfide Glass Electrolytes. *J. Mater. Chem. A* **2015**, *3*, 22061–22065.

(27) Homma, K.; Yonemura, M.; Kobayashi, T.; Nagao, M.; Hirayama, M.; Kanno, R. Crystal Structure and Phase Transitions of the Lithium Ionic Conductor Li_3PS_4. *Solid State Ionics* **2011**, *182*, 53–58.

(28) Vineyard, G. H. Frequency Factors and Isotope Effects in Solid State Rate Processes. *J. Phys. Chem. Solids* **1957**, *3*, 121–127.

(29) Toyoura, K.; Koyama, Y.; Kuwabara, A.; Oba, F.; Tanaka, I. First-principles Approach to Chemical Diffusion of Lithium Atoms in a Graphite Intercalation Compound. *Phys. Rev. B* **2008**, *78*.

(30) Jansen, M. Volumeneffekt oder Drehtürmechanismus - Schnelle Alkalimetall-Ionenleitung in Festkörpern mit Rotationsfehlgeordneten Komplexen Anionen. *Angew. Chem.* **1991**, *103*, 1574–1586.

(31) Wilmer, D.; Funke, K.; Witschas, M.; Banhatti, R. D.; Jansen, M.; Korus, G.; Fitter, J.; Lechner, R. E. Anion Reorientation in an Ion Conducting Plastic Crystal - Coherent Quasielastic Neutron Scattering from Sodium Ortho-phosphate. *Physica B* **1999**, *266*, 60–68.

(32) Rao, R. P.; Adams, S. Studies of lithium argyrodite solid electrolytes for all-solid-state batteries. *Phys. Status Solidi A* **2011**, *208*, 1804–1807.

(33) Chen, H. M.; Chen, M.; Adams, S. Stability and Ionic Mobility in Argyrodite-related Lithium-ion Solid Electrolytes. *Phys. Chem. Chem. Phys.* **2015**, *17*, 16494–16506.

Table of Contents figure